Computational and Structural Biotechnology Journal 17 (2019) 498–506

COMPUTATIONAL AND STRUCTURAL BIOTECHNOLOGY JOURNAL

journal homepage: www.elsevier.com/locate/csbj

Mouse-Derived Allografts: A Complementary Model to the KPC Mice on Researching Pancreatic Cancer In Vivo

Jie Li [1], Weikun Qian [1], Tao Qin, Ying Xiao, Liang Cheng, Junyu Cao, Xin Chen, Qingyong Ma *, Zheng Wu *

Department of Hepatobiliary Surgery, First Affiliated Hospital of Xi'an Jiaotong University, Xi'an 710061, China

ARTICLE INFO

Article history:
Received 9 November 2018
Received in revised form 29 March 2019
Accepted 30 March 2019
Available online 6 April 2019

Keywords:
Pancreatic ductal adenocarcinoma
Mouse-derived allografts
Tumor tissue fragment
Gemcitabine

ABSTRACT

Pancreatic ductal adenocarcinoma (PDAC) is one of the most malignant cancers and has an extremely undesirable prognosis because little is known about the initiation and progression mechanisms of pancreatic cancer. The lack of an appropriate research model may have hindered this process. Using *LSL-Kras*$^{G12D/+}$; *Trp53*$^{fl/+}$; *Pdx1-Cre* (KPC) mice and the tumor tissue fragment transplantation technique, we constructed the mouse-derived subcutaneous/orthotopic allograft tumor models (MDAs-ST/OT). H&E staining, Masson staining and immunohistochemical staining were adopted to describe the histopathology and biomarkers of the MDAs and the recruitment of immune cells. The intervention of gemcitabine was applied to measure the chemotherapeutic response of MDAs tumors. MDAs could mimic the pathological histology and the high proliferation characteristics of PDAC. Indeed, the fibrosis, epithelial-mesenchyme transition (EMT) and invasion/metastasis related markers of MDAs were similar to those observed in pancreatic cancer. Further, the recruitment of immune cells in PDAC was precisely simulated by MDAs. In addition, gemcitabine suppressed the tumor growth of MDAs-ST significantly. MDAs are an effective model for investigating the progression and treatment of pancreatic cancer.

1. Introduction

Pancreatic ductal adenocarcinoma (PDAC) is one of the most malignant tumors and has a 5-year survival rate <8% [1]. Most patients are diagnosed at an advanced stage, so they cannot undergo radical surgery. However, even for those who receive a complete surgical resection, the 5-year survival is still approximately 25%. For these patients, many chemotherapy options such as gemcitabine, S-1(an oral fluoropyrimidine derivative), FOLFIRINOX (fluorouracil, folinic acid, irinotecan, and oxaliplatin) or gemcitabine plus nanoparticle albumin-bound paclitaxel (nab-paclitaxel) could adopted instead [2,3]. Nevertheless, these therapeutic strategies do not provide a good clinical outcome for some patients. The reasons for these poor statuses may be due to the poor understanding of the initiation, progression and therapy mechanisms of PDAC. Notably, the lack of an appropriate in vivo model may be the main factor restricting the research into the mechanisms of PDAC.

Researchers have developed and studied numerous in vivo models of PDAC, for example, pancreatic cancer cell sources of subcutaneous/orthotopic transplantation tumor and their correlation techniques [4,5], patient-derived subcutaneous/orthotopic xenografts (PDXs) and their correlation techniques [6] and various genetically engineered mouse models (GEMMs) and organoid models of pancreatic cancer [7,8]. The use of the in vivo models mentioned above provides great convenience for the progression of pancreatic cancer research. However, to some extent, the above processes are limited; for example, the immunodeficient status of transplant tumor models does not reflect the real growth environment of pancreatic cancer.

Abbreviation: PDAC, Pancreatic ductal adenocarcinoma; GEMMs, Genetically engineered mouse models; KC, *LSL-Kras*$^{G12D/+}$, *Pdx1-Cre*; KPC, *LSL-Kras*$^{G12D/+}$, *Trp53*$^{fl/+}$, *Pdx1-Cre*; MDAs, Mouse-derived allografts; MDAs-ST, Mouse-derived subcutaneous allograft tumor models; MDAs-OT, Mouse-derived orthotopic allograft tumor models; PDXs, Patient-derived xenografts; ADM, Acinar to ductal metaplasia (ADM); PanINs, Pancreatic intraepithelial neoplasias; CAFs, Cancer-associated fibroblasts; EMT, Epithelial-mesenchyme transition; MDSCs, Myeloid-derived suppressor cells; Tregs, T regulatory cells.

* Corresponding authors.
E-mail addresses: lijiel@stu.xjtu.edu.cn (J. Li), qianweikun@stu.xjtu.edu.cn (W. Qian), qintao31zongjian@stu.xjtu.edu.cn (T. Qin), zxj6988@stu.xjtu.edu.cn (Y. Xiao), qyma56@xjtu.edu.cn (Q. Ma), wuzheng@xjtu.edu.cn (Z. Wu).
[1] Co-first authors.

https://doi.org/10.1016/j.csbj.2019.03.016

To overcome the deficiencies mentioned above and provide an appropriate in vivo model of pancreatic cancer, in this study, using a GEMM of pancreatic cancer named *LSL-Kras*$^{G12D/+}$; *Trp53*$^{fl/+}$; *Pdx1-Cre* (KPC) mice [9], we developed novel in vivo models of pancreatic cancer termed mouse-derived subcutaneous/orthotopic allograft tumor models (MDAs-ST/OT).

2. Methods and Materials

2.1. Genetically Engineered Mouse Models

The GEMMs of pancreatic cancer [10,11], *LSL-Kras*$^{G12D/+}$ (K) mice (B6.129S4-K-rastm4Tyj/NJU), *Trp53*$^{fl/+}$ (P) mice (FVB.129-Trp53 < tm1Brn>) and *Pdx1-Cre* (C) mice (B6.FVB-Tg(Ipfl-cre)1Tuv) were acquired from the Nanjing Biomedical Research Institute of Nanjing University, Nanjing, China. To obtain KPC mice, we first crossed *LSL-Kras*$^{G12D/+}$mice with *Trp53*$^{fl/+}$ mice to produce *LSL-Kras*$^{G12D/+}$; *Trp53*$^{fl/+}$ (KP) mice; subsequently, *Pdx1-Cre* mice were crossed with KP mice to generate KPC (*LSL-Kras*$^{G12D/+}$; *Trp53*$^{fl/+}$; *Pdx1-Cre*) mice (a mixed 129/FVB/C57BL/6 background). Notably, in the process of hybridization, we also obtain syngeneic wild type (WT) mice (*Kras*$^{+/+}$; *Trp53*$^{+/+}$; *Pdx1-Cre*$^{-/-}$). All mice were reared in a specific pathogen-free environment, with the temperature controlled at 24 °C and a 12-h/12-h light/dark cycle at the Experimental Animal Center of Xi'an Jiaotong University, Xi'an, China. A UV lamp installed in the pathogen-free chamber was used to maintain sterile conditions. There was also a buffer room between the pathogen-free chamber and the room in which the KPC mice were reared. The food, water, and bedding used by the KPC mice were sterilized. All experimental protocols were approved by the Ethics Committee of the First Affiliated Hospital of Xi'an Jiaotong University, Xi'an, China.

2.2. The Establishment of the Mouse-Derived Subcutaneous/Orthotopic Allografts

We harvested PDAC tumor tissue from 6 KPC mice named KPC 1–6 (KPC 1: survival time 132 days, tumor volume 17 × 12 × 6 mm, tumor weight 1.32 g; KPC 2: survival time 127 days, tumor volume 14 × 13 × 5 mm, tumor weight 1.28 g; KPC 3: survival time 129 days, tumor volume 18 × 12 × 6 mm, tumor weight 1.36 g; KPC 4: survival time 137 days, tumor volume 16 × 11 × 6 mm, tumor weight 1.26 g; KPC 5: survival time 125 days, tumor volume 14 × 10 × 7 mm, tumor weight 1.22 g; KPC 6: survival time 135 days, tumor volume 17 × 11 × 7 mm, tumor weight 1.28 g). Then, the tissues were trimmed and washed in 0.9% NaCl, and each was placed into 4 °C RPMI-1640 medium immediately. Subsequently, they were cut into fragments of approximately 3 × 3 × 3 mm for transplantation (we replaced the 4 °C RPMI-1640 medium at least 3 times each to maintain a good storage environment for these tumor tissue fragments).

To establish MDAs, we first used 4% chloral hydrate (0.1 ml/20 g) to anesthetize WT mice (4 weeks old) and then shave their hair. Second, we used aseptic operation to put the tumor tissue fragments into the neck subcutaneous tissue or orthotopically into the pancreas tissue of WT mice. Finally, we resuscitated the WT mice and monitored their behavior. Tumor tissue fragments from each of KPC 1–3 were transplanted into the neck subcutaneous tissue (12 WT mice) and orthotopically into the pancreatic tissue (12 WT mice) to monitor the growth rate of the tumor. Tumor tissue fragments from KPC 4 were transplanted into the neck subcutaneous tissue and orthotopically into the pancreatic tissue of 24 WT mice to compare the growth of subcutaneous and orthotopic tumors. Tumor tissue fragments from KPC 5 were transplanted into the neck subcutaneous tissue of 12 WT mice and 12 BALb/c nude mice (4 weeks old, female, supplied by and housed in the Animal Center at Medical College, Xi'an Jiaotong University). Tumor tissue fragments from KPC 6 were transplanted into the neck subcutaneous tissue of 24 WT mice and divided them into two groups: control (saline, 0.1 ml/mice, i.p. every 3 days) vs gemcitabine (100 mg/kg, i.p. every 3 days) randomly. The above procedures shall follow the principle of aseptic operation.

We measured the tumor volume of MDAs-ST (Length × Width^2/2) and the weight of WT mice every 3 days. The entire observation period lasted 4 weeks. At the end of the observation, we euthanized the mice and harvested the pancreas and tumor tissues of the MDAs. The tissues were fixed in 10% buffered formalin and embedded in paraffin immediately for hematoxylin & eosin (H&E) staining, immunohistochemical (IHC) staining and Masson trichrome staining.

2.3. Immunohistochemistry

IHC staining was performed using SABC kits (Maxim, Fuzhou, China) according to the manufacturer's instructions. In brief, the pancreas or tumor tissue sections were incubated with primary antibodies against the following antigens: CD68, CD3, MPO, VEGF, CD31, E-cadherin, N-cadherin, Vimentin, MMP2/9 (Servicebio, Wuhan, Hubei, China) and Ki67, α-SMA, amylase, CK19 (Abcam, Cambridge, MA, USA) overnight at 4 °C. The sections were incubated with the appropriate biotinylated secondary antibody for 30 min at room temperature, followed by 30 min of incubation with streptavidin peroxidase (Dako, Glostrup, Denmark, LSAB + HRP kit). After rinsing, the antigen signals were visualized using DAB, and the slides were counterstained with hematoxylin. Five fields (400 ×) were randomly selected from each slide, and the proportion of the positive area in each field was determined using a true color multi-functional cell image analysis management system (Image-Pro Plus version 6.0; Media Cybernetics, Silver Springs, MD, USA).

2.4. Micro-Vessel Density/Count Analysis (MVD)

MVD analysis [12] was adapted to measure the tumor angiogenesis of PDAC by staining for the vascular endothelial cell marker, CD31. Briefly, without knowledge of the origin of the tissue, we used low-power (100×) magnification to determine the highest neovascularization area of the tumor tissue sections. A 400 × magnification was adopted to count the clearly identifiable micro-vessels among cancer cells and other elements in the field. Five fields (400×) were randomly selected from each slide, and each count was expressed as the highest number of micro-vessels.

2.5. Masson Trichrome Staining

Masson trichrome staining was performed using a kit from Sigma-Aldrich (St. Louis, MO, USA) according to the manufacturer's protocol. Five fields (400×) were randomly selected from each slide, and the proportion of the positive area in each field was determined using a true color multi-functional cell image analysis management system (Image-Pro Plus version 6.0; Media Cybernetics).

2.6. Statistical Analysis

The data are presented as mean ± SD. Using the GraphPad Prism software package (GraphPad Prism version 6.0; La Jolla, CA, USA), differences in the in vivo data were assessed by Student's *t*-test or one-way ANOVA. All tests were two-sided, and statistical significance was declared based on a P value <0.05.

3. Results

3.1. The Build Process and Tumor Growth of the MDAs

We adopted 4 KPC mice as the transplant donors and a number of WT mice as the transplant recipients. As mentioned above, we first excised the PDAC tumor tissues of KPC mice and cut them into fragments of approximately 3 × 3 × 3 mm. We transplanted these tissue fragments

into the neck subcutaneous tissue or orthotopically into the pancreatic tissue of WT mice and observed the tumor growth and living behavior of these mice (Fig. 1A). We also measured the tumor growth of MDAs-ST. The results showed that after the 7th day of transplantation, MDAs-ST derived from all KPC 1–3 grew more rapidly than at other times (Fig. 1B). However, the weights of WT mice showed no obvious change in both MDAs-ST and MDAs-OT (data not show). We also compared the tumor growth of MDAs-ST with MDAs-OT weekly and concluded that tumors of MDAs-OT grew faster than MDAs-ST did at every time point, which was verified by the tumor volume and number of Ki67 positive cells (Fig. 1C,D). In conclusion, we successfully established MDAs as stable and rapid tumor models of pancreatic cancer.

3.2. The Macroscopic and Microscopic Morphology of MDAs

KPC mice are valuable GEMMs of pancreatic cancer and can mimic the sequential developmental process of human PDAC from normal acinar cells to acinar to ductal metaplasia (ADM), pancreatic intraepithelial neoplasias (PanINs) and invasive PDAC vividly (Fig. 2A). Interestingly, both MDAs-ST and MDAs-OT can mimic the macroscopic morphology (a quasi-spherical, gray and hard outlook) and microscopic architectural/cytologic changes of PDAC: the loss of acinar and/or ductal architecture, which is replaced by the formation of excessive abnormal ductal-like structures, the clear cellular and nuclear atypia, and many aberrantly located cellular compartments [13] (Fig. 2B). Additionally, the tumors in MDAs-OT were larger than those in MDAs-ST for all 3 sources (Fig. 2B). These data suggested that MDAs are suitable models of pancreatic cancer from the pathological perspective.

3.3. The Molecular Markers of MDAs

There is a consensus that PDAC have many alterations in their histology, biomarkers and signaling pathways compared with normal pancreas [13,14]. We already demonstrated the architectural/cytological changes of MDAs, so we next examined some common biomarkers and interstitial changes of MDAs. Using IHC staining, we first tested the expression of the acinar marker amylase and ductal marker CK19 in PDAC of KPC mice, normal pancreatic tissues, and subcutaneous/orthotopic tumor tissues of MDAs. The results show that compared to normal pancreatic tissues, tumor tissues from both PDAC and MDAs have a clear loss of acinar phenotype; however, a distinct gain of ductal

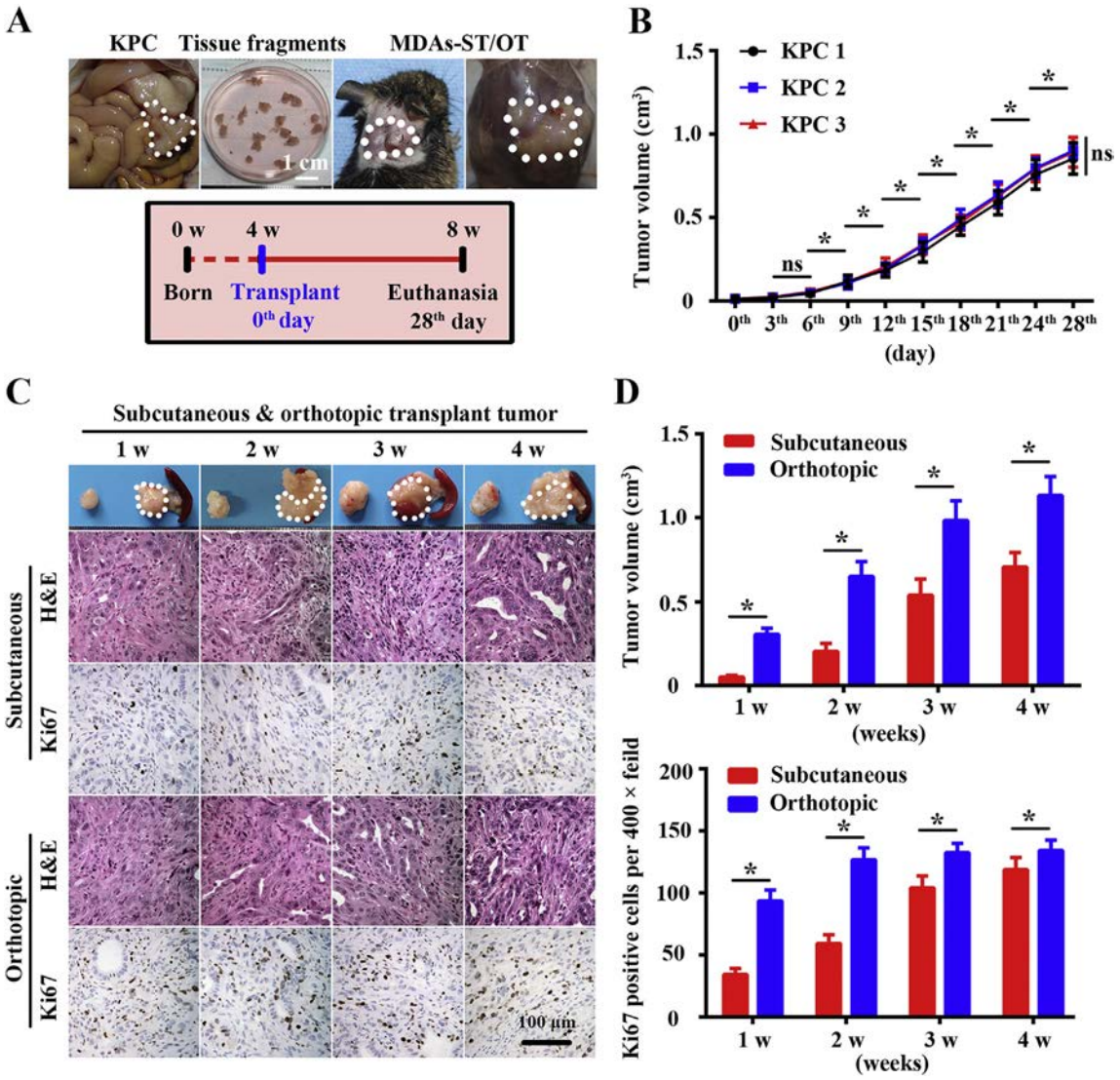

Fig. 1. The creation process and tumor growth of MDAs. (A) Diagram of the creation process of MDAs. (B) The tumor growth curve of MDAs-ST derived from KPC 1–3. (C) Representative photomicrographs of H&E staining and IHC staining of Ki67 positive cells in tumor tissues of MDAs-ST/OT collected weekly. (D) The comparison of the tumor volume of MDAs-ST/OT and the quantification of Ki67-positive cells per 400 × field. Scale bars =100 μm. ns $P > 0.05$, *$P < 0.05$.

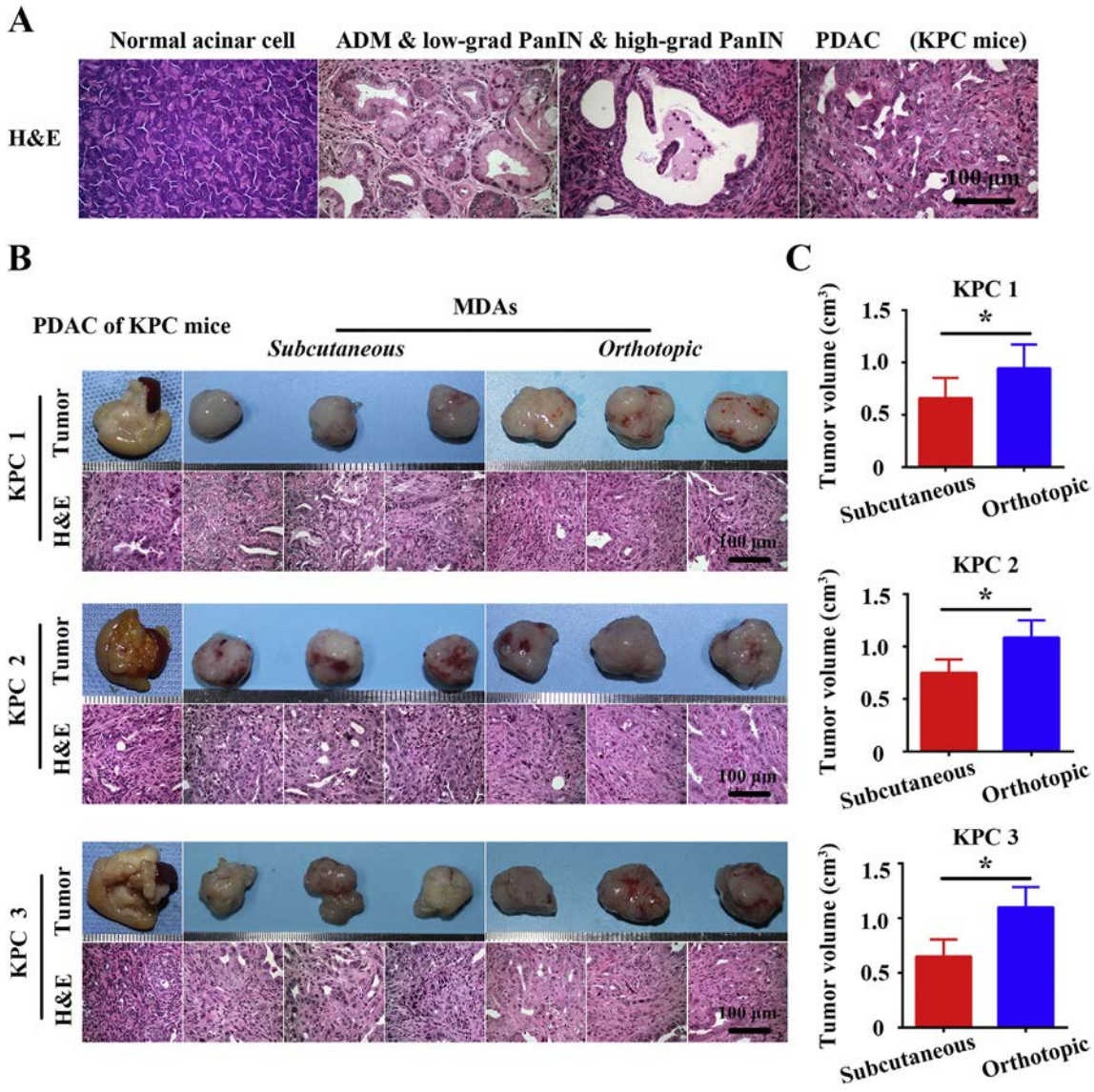

Fig. 2. The macroscopic and microscopic morphology of MDAs. (A) Representative histopathology of the normal pancreas and pancreatic cancer or its precursor lesions in KPC mice. (B) Representative macroscopic and microscopic images of PDAC tumor tissues in KPC 1–3 and its corresponding offspring MDAs tumor tissues. (C) The comparison of the tumor volume of MDAs-ST/OT. Scale bars = 100 μm. *P < 0.05.

phenotype was observed (Fig. 3A,C). Similarly, the proliferation of tumor tissues in both PDAC and MDAs was higher than that of normal pancreatic tissues (Fig. 3A,B). Next, Masson and IHC staining showed the interstitial changes of pancreatic cancer. Compared to normal tissues, the desmoplastic reaction and angiogenesis in the tumor tissue from both PDAC and MDAs were more robust (Fig. 4). Finally, we measured the epithelial-mesenchyme transition (EMT) and invasion/metastasis-related markers of MDAs, and we found consequences similar to the above results (Fig. 5). These results indicated that those MDAs could simulate the biomarker changes of PDAC, which means that these models can be used in pancreatic cancer research.

3.4. The Immune Cell Infiltration of MDAs

Substantial evidence has supported the pathologic role of the immune cells and inflammatory microenvironment in pancreatic cancer [11,15,16]. One of the great advantages of MDAs is its intact immune system. Therefore, we measured the immune cell infiltration in MDAs and found higher numbers of MPO-positive cells, which represent neutrophils or their precursors in the stroma of tumor tissues of PDAC and MDAs compared to normal pancreatic tissues. In addition, we found high numbers of CD68-positive macrophages; however, fewer CD3-positive T cells were observed in all three tissues (Fig. 6A,B), which indicates the formation of an immunosuppressive microenvironment in both PDAC and MDAs. Further, to explore the role of immune microenvironment on the growth of tumor, we transplanted the KPC tumor tissue fragments into the neck subcutaneous tissue of WT mice (immunocompetent MDAs) and nude mice (immunodeficient MDAs), and we found that the growing speeds were quite different in these two kinds of MDAs (Fig. 6C,D). Indeed, we measured the tumor associated immunosuppressive cell infiltration in these two kinds of MDAs and found higher numbers of MPO-positive neutrophils, Gr.1-positive myeloid-derived suppressor cells (MDSCs) and CD206-positive M2 macrophages in the stroma of tumor tissues WT mice compared to nude mice, which means immunocompetent WT mice formed a severer tumor immunosuppressive microenvironment than immunodeficient nude mice. Interestingly, there were few FoxP3-positive T regulatory cells (Tregs) in WT mice tumor tissues and no Tregs in nude mice tumor tissues (T cell function is defective in nude mice) (Fig. 6E,F). These findings proved that our established immunocompetent MDAs are remarkable tools in studying the cross-talk between pancreatic cancer and the immune system.

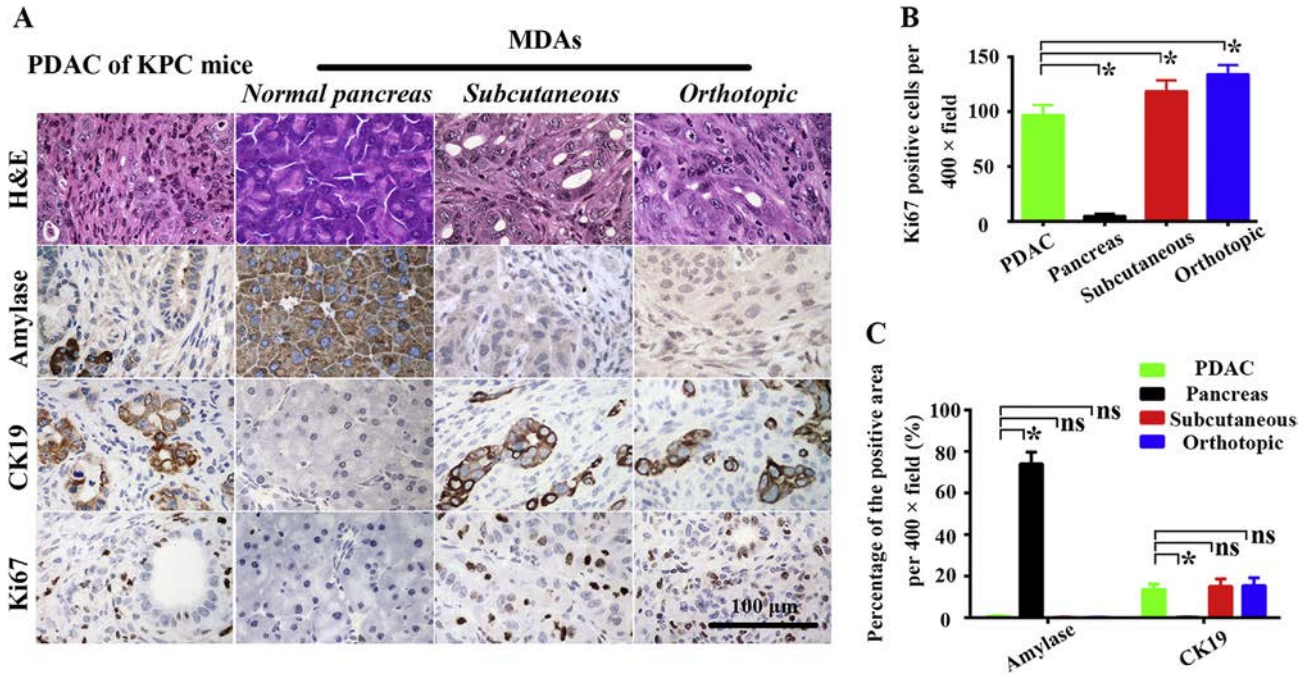

Fig. 3. The histopathology, acinar marker, ductal marker and proliferation marker of MDAs. (A) Representative photomicrographs of H&E staining and IHC staining of amylase (acinar marker), CK19 (ductal marker) and Ki67 (proliferation marker) of PDAC in KPC mice, normal pancreatic tissues and subcutaneous/orthotopic tumor tissues of MDAs. (B) Quantification of Ki67-positive cells per 400 × field. (C) Quantification of the percentage of the amylase/CK19-positive area per 400 × field (%). Scale bars = 100 μm. ns $P > 0.05$, *$P < 0.05$.

3.5. Gemcitabine Suppressed the Tumor Growth of MDAs

Although a certain of drug resistance is existing, gemcitabine is still regard as the first line and irreplaceable treatment for PDAC in the present [17]. Interestingly, we created the MDAs which can mimic the pathological feature of PDAC vividly. Hence, we next use gemcitabine to verify whether MDAs could mimic the chemotherapeutic response of PDAC. We first used another PDAC tumor tissues of KPC mice (KPC 6) to create MDAs-ST and divided them into two therapeutic group (control vs gemcitabine); as we mentioned above, a significant increase in the size of the tumor of MDAs-ST occurred in 7th days after transplanted, so we started the intervention at this time and lasted for

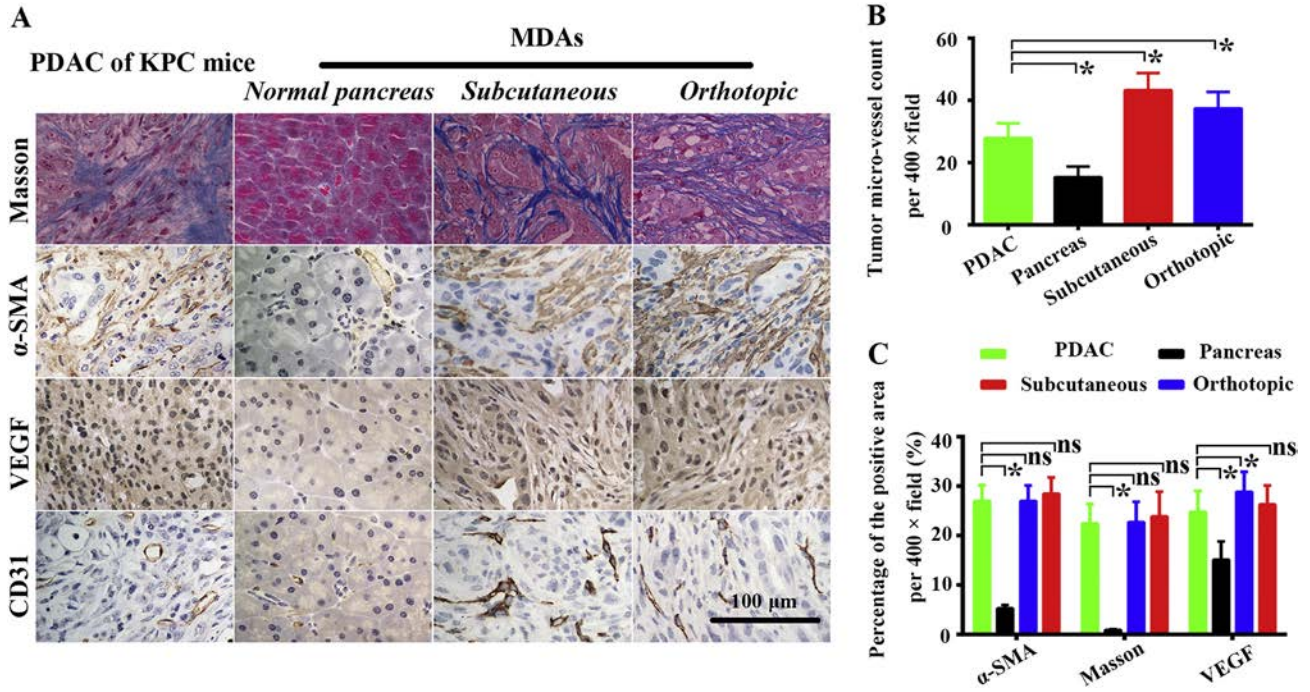

Fig. 4. The desmoplastic reaction and angiogenesis of MDAs. (A) Representative photomicrographs of Masson staining and IHC staining of α-SMA, VEGF and CD31 of PDAC in KPC mice, normal pancreatic tissues, and subcutaneous/orthotopic tumor tissues of MDAs. (B) Quantification of the tumor micro-vessel count per 400 × field. (C) Quantification of the percentage of the α-SMA/VEGF/Masson-positive area per 400 × field (%). Scale bars =100 μm. ns $P > 0.05$, *$P < 0.05$.

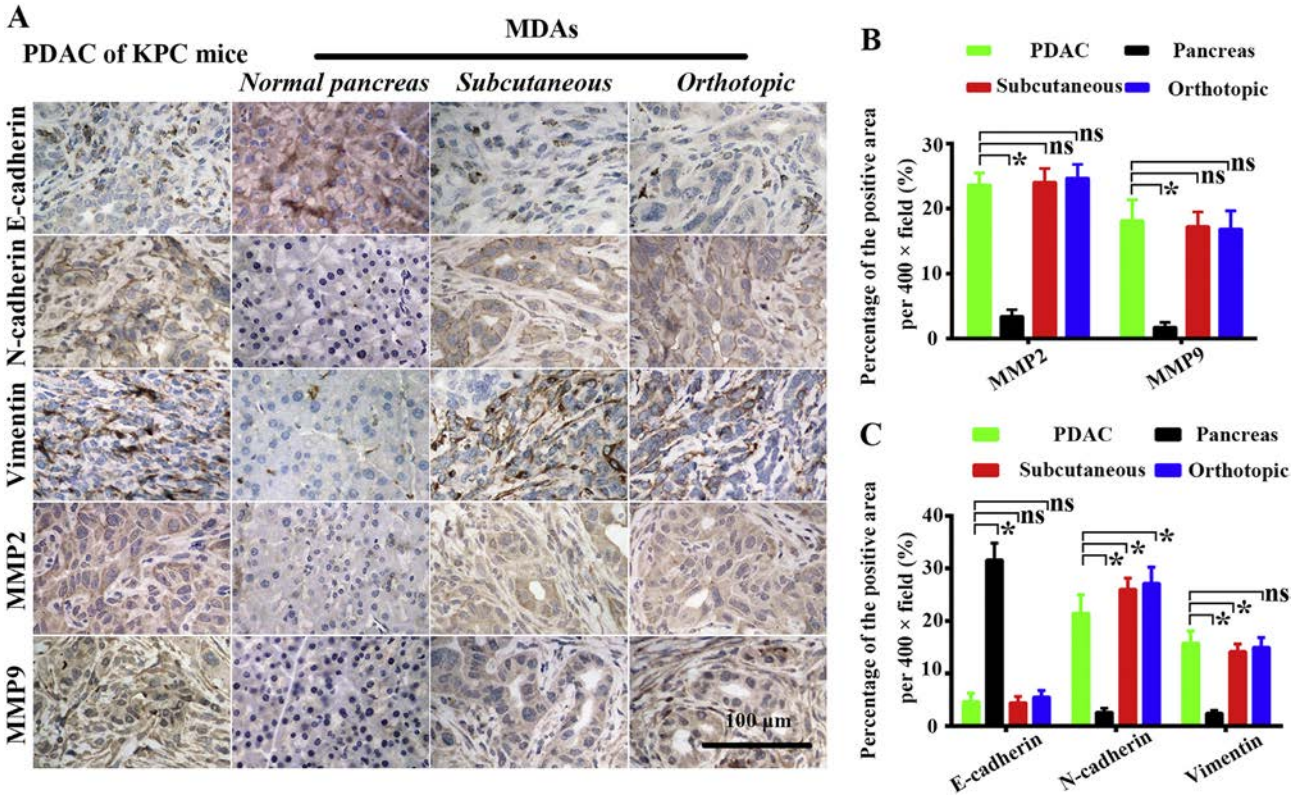

Fig. 5. The epithelial-mesenchyme transition and invasion/metastasis-related markers of MDAs. (A) Representative photomicrographs of IHC staining of E-cadherin, N-cadherin, Vimentin and MMP2/9 of PDAC in KPC mice, normal pancreatic tissues and subcutaneous/orthotopic tumor tissues of MDAs. (B) Quantification of the percentage of the MMP2/9-positive area per 400 × field (%). (C) Quantification of the percentage of the E-cadherin/N-cadherin/Vimentin-positive area per 400 × field (%). Scale bars = 100 μm. ns $P > 0.05$, *$P < 0.05$.

3 weeks; besides, we repeated above strategy on MDAs-OT (Fig. 7A). We then monitored the tumor growth of MDAs-ST during the observation period and the results showed that gemcitabine suppressed the tumor growth of MDAs-ST significantly (Fig. 7D,E). Finally, we counted the number of Ki67-positive cells in tumor tissues of both control and gemcitabine group and the results showed that gemcitabine suppressed the tumor cell proliferation of MDAs-ST obviously (Fig. 7B,C). However, by using MDAs-OT, we found no difference between control and gemcitabine group on tumor volume and Ki67-positive proliferation cells (Fig. 7F–H). In summary, MDAs-ST are better tools on researching the chemotherapeutic response of PDAC.

4. Discussion

PDAC is a highly malignant disease with a poor prognosis worldwide [1,18]. An appropriate in vivo model could help researchers solve this dilemma. Hence, many in vivo models have been developed. The most widely used in vivo model is the pancreatic cancer cell source subcutaneous/orthotopic transplantation tumor model; however, it cannot reflect the interactions between stromal elements with pancreatic cancer cells. Therefore, our research group usually adopted an improved transplant model in which subcutaneous/orthotopic co-injection with pancreatic cells and pancreatic stellate cells into nude mice could partly solve the above problem [5,19]. Nevertheless, except for cancer-associated fibroblasts (CAFs) and the dense desmoplastic tumor stroma derived from them, the pancreatic cancer tumor microenvironment includes other components such as vascular endothelial cells, inflammatory cells and many non-cellular components [20–23]. Besides, tumor microenvironment in pancreatic cancer not only promotes tumor initiation and progression but also mediates therapeutic resistance [24]. Indeed, whole-genome sequencing data show that the heterogeneity of pancreatic cancer was ubiquitous [25]. Hence, we concluded that single cellular transplant tumor models cannot overcome these deficiencies fundamentally. Therefore, PDXs and its related models were established [6] that can reflect the tumor microenvironment and the heterogeneity of pancreatic cancer, but their disadvantages include the high requirements for transplant donors, the complexity of the surgery and the immunodeficient status of the transplant recipient. Currently, GEMMs are considered the most valuable in vivo models of pancreatic cancer because of their irreplaceable advantages in studying PDAC initiation, progress, metastasis, and therapy [8,26]. However, their high cost, the complexity of their establishment and the rarity of terminal mice limits their large-scale application [27].

Studies have shown that *Kras*, which is often called "the molecular switch", is the most common and pivotal mutated gene in the initiation and progression of PDAC; *Kras* mutations occur in >90% of patients with PDAC [28]. Additionally, somatic mutations in the *p53* tumor suppressor gene are frequent genetic events that drive PDAC progression [29]. The above observations prompted the development of *LSL-Kras*$^{G12D/+}$; *Pdx1-Cre* (KC) mice and *LSL-Kras*$^{G12D/+}$; *Trp53*^{R172H}/*Trp53*$^{fl/+}$; *Pdx1-Cre* (KPC) mice to become the most common use GEMMs of PDAC [9,30,31]. Hence, in this work, to overcome the disadvantages of GEMMs in studying PDAC, we used KPC mouse pancreatic cancer tumor tissues and WT mice to create MDAs. The results showed that MDAs could mimic the progression of PDAC accurately (both in histopathology and biomarkers). Specifically, tumors in MDAs-ST grew in a faster rate after the 7th day of transplantation (this phenomenon may be related to the tumor angiogenesis and the interaction of tumor cells with the host immune system). The entire experimental cycle was short at one month, which makes it suitable for studying the growth inhibition effect of small molecule inhibitors or even medicinal extracts against PDAC. As we can see, by using gemcitabine (the first line treatment of PDAC [17,32]), tumor growth of MDAs-ST was suppressed significantly in a one-month observation period. Nevertheless, researches have proven that gemcitabine have limitation benefits in clinical because of the chemo-resistant and the curative effect of many new treatment options

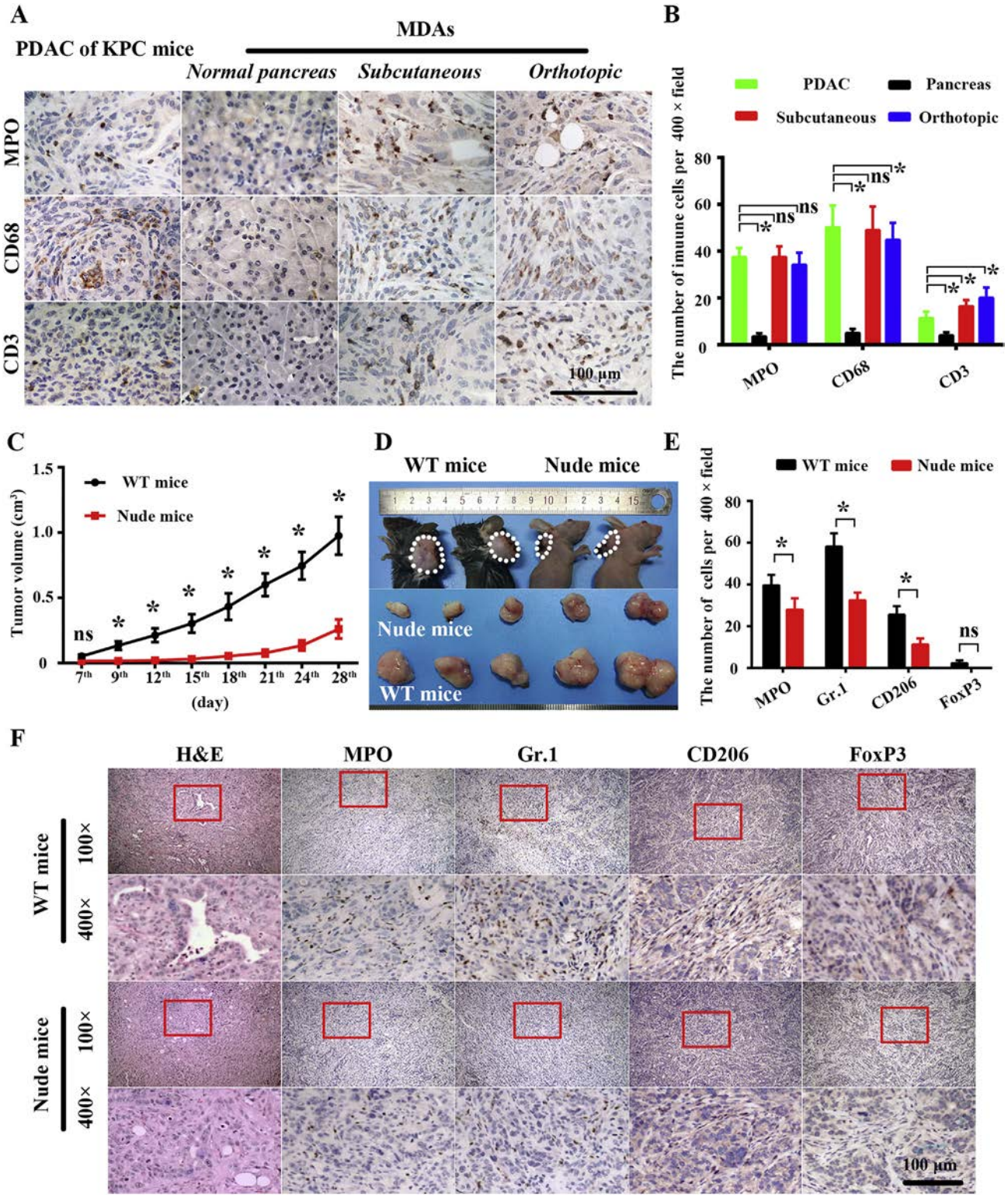

Fig. 6. The immune cell infiltration of MDAs. (A) Representative photomicrographs of IHC staining of MPO (neutrophils marker), CD68 (macrophages marker) and CD3 (T cell marker) of PDAC in KPC mice, normal pancreatic tissues and subcutaneous/orthotopic tumor tissues of MDAs. (B) Quantification of MPO/CD68/CD3-positive cells per 400 × field. (C) The subcutaneous transplant tumor growth curve of WT mice and nude mice. (D) Representative macroscopic of subcutaneous transplant tumor of WT mice and nude mice. (E) Quantification of MPO/Gr.1/CD206/FoxP3-positive cells per 400 × field. (F) Representative photomicrographs of H&E staining and IHC staining for MPO (neutrophils marker), Gr.1 (MDSCs marker), CD206 (M2 macrophages marker) and FoxP3 (Tregs marker). Scale bars = 100 μm. ns $P > 0.05$, $^{*}P < 0.05$.

such as S-1, FOLFIRINOX or gemcitabine plus nanoparticle albumin-bound paclitaxel were better than gemcitabine [3,33,34]. Indeed, by using a similar orthotopic and heterotopic murine models of pancreatic cancer, Erstad DJ and colleagues demonstrated that FOLFIRINOX chemotherapy benefited to the pancreatic cancer in GEMMs [35]. This discrepancy may because that we treated the MDAs-ST with gemcitabine when the tumor was still small (similar to the early stage of pancreatic cancer in clinical, in this stage, the perfusion of gemcitabine was enough and pancreatic cancer cells were sensitivity to gemcitabine [34]).Hence, in future studies, gemcitabine treatment

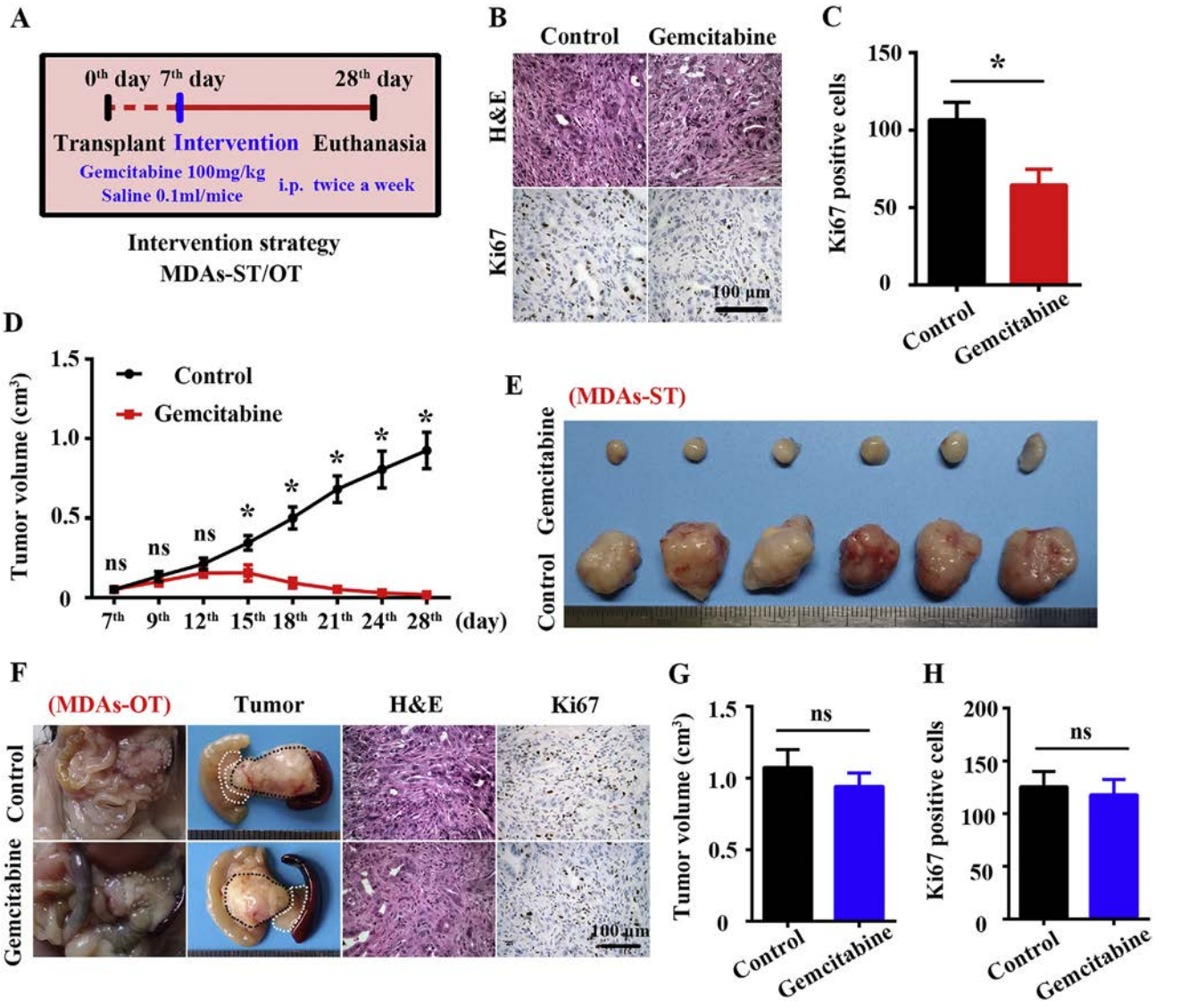

Fig. 7. Gemcitabine suppressed the tumor growth of MDAs. (A) Diagram of the intervention strategy of gemcitabine on MDAs-ST/OT. (B) Representative photomicrographs of H&E staining and IHC staining of Ki67 positive cells in tumor tissues of both control and gemcitabine group (MDAs-ST). (C) The comparison of the Ki67-positive cells per 400 × field between control group and gemcitabine group (MDAs-ST). (D) The tumor growth curve of control group and gemcitabine group (MDAs-ST). (E) Representative macrograph of tumors in both control and gemcitabine group (MDAs-ST). (F) Representative macrograph (white dashed box means normal pancreas, gray dashed box means squeezed pancreas, black dashed box means transplant tumor tissue), photomicrographs of H&E staining and IHC staining of Ki67 positive cells of tumors in both control and gemcitabine group (MDAs-OT). (G) The tumor growth curve of control group and gemcitabine group (MDAs-OT). (H) The comparison of the Ki67-positive cells per 400 × field between control group and gemcitabine group (MDAs-OT). Scale bars =100 μm. ns $P > 0.05$, *$P < 0.05$.

should start when tumors are bigger and the observation period should be prolong, what's more, new therapeutic strategies should also be adopted to further validate/evaluate the value of this model on screening chemotherapeutic drug. Different to MDAs-ST, MDAs-OT tumors grow rapidly at all stages, and we found the anti-tumor effect of gemcitabine party weaken in MDAs-OT, which may because that the growth environment of MDAs-OT tumors was closer to that of spontaneous pancreatic cancer. In this environment, pancreatic cancer cells proliferate severely and tumor grow rapidly, when we started gemcitabine intervention, orthotopic transplant tumors is big enough to confront the killing effect of gemcitabine. Moreover, by using a novel fluorescently-labeled orthotopic PDXs, researchers found the host fibroblast infiltrated into the donor tumor tissues; together with other stromal elements, they formed a new tumor microenvironment, which promoted tumor progression and metastasis [6]. In our view, the nature of the tumor can change due to new interactions of the tumor cells with new fibroblasts with different genetic and phenotypic alterations, and orthotopic transplant tumors can recruit adjacent pancreas fibroblast (such as CAFs) and other elements easier and then form a more realistic tumor microenvironment (such as abundant desmoplastic reaction) compare with MDAs-ST, which promotes the rapid progression of tumors and waken the anti-tumor effect of gemcitabine. Hence, we can use these tumors to explore the molecular mechanisms of rapid proliferation, invasion and metastasis of PDAC as well as the cross-talk between tumor cells to surrounding microenvironment and lots of studies needs to be done. Besides, the advantages of MDAs-OT are its low cost, the controllability of the number of the mice and the homogeneity of the findings compared to KPC mice, however, the real-time monitoring of the tumor growth was the challenge of both KPC mice and MDAs-OT, which restrict the use of it. Mentionablely, the host of our established MDAs was immunocompetent WT mice, which means it can mimic the interaction between immune system and pancreatic cancer more vividly than traditional immunodeficient transplantation tumor models. Researches has supported the pathologic

role of the immune microenvironment in pancreatic cancer and our established MDAs can simulate the infiltrate of immune cell in spontaneous PDAC effectively [11]. Indeed, we found that tumor in immunocompetent WT mice grew faster than in immunodeficient nude mice, and these may partly due to the severer tumor immunosuppressive microenvironment in immunocompetent WT mice the severer tumor immunosuppressive microenvironment in immunocompetent WT mice [36]; specifically, WT mice tumor tissues has higher tumor associated immunosuppressive cells infiltrated such as MPO+ neutrophils, Gr.1+ MDSCs, CD206+ M2 macrophage and FoxP3+ Tregs [37–40], which means WT mice formed a severer tumor promotion immunosuppressive microenvironment than immunodeficient nude mice.These findings highlight the role of our established immunocompetent MDAs in studying the cross-talk between pancreatic cancer and the immune system.

Notably, we cultured and subcultured MDAs for at least 7 successive generations to explore the changes on the histopathology and biomarkers of MDAs tumors (data not show). However, the largest limitation of MDAs is the need of a mature master on KPC mice; further, we have not clearly illustrated the specific signal pathways related to the tumor progression of MDAs. Hence, a large amount of work should be done to make MDAs an outstanding pancreatic cancer in vivo model.

5. Conclusion

MDAs mimic the pathological histology and the various biological characteristics of PDAC in an immunocompetent organism. Meanwhile, MDAs make up for the deficiencies of KPC mice which make it to be a valuable supplement of KPC on the research of the progression of pancreatic cancer.

Author Contributions

JL (Jie Li), WQ (Weikun Qian), ZW (Zheng Wu) and QM (Qingyong Ma) designed the experiments. JL (Jie Li), WQ (Weikun Qian), TQ (Tao Qin) and YX (Ying Xiao) performed the majority of the experiments. LC (Cheng Liang) and JC (Junyu Cao) analyzed the data. XC (Xin Chen) organized the figures and were involved in the conception of the study. JL (Jie Li), WQ (Weikun Qian) wrote the manuscript. ZW (Zheng Wu) and QM (Qingyong Ma) reviewed the manuscript and supervised this study.

Declaration of Interest

None.

Acknowledgements

This study was supported by grants from the National Natural Science Foundation of China (81672434).

References

[1] Siegel RL, Miller KD, Jemal A. Cancer statistics, 2017. CA Cancer J Clin 2017;67(1):7–30.
[2] Uesaka K, Boku N, Fukutomi A, et al. Adjuvant chemotherapy of S-1 versus gemcitabine for resected pancreatic cancer: a phase 3, open-label, randomised, non-inferiority trial (JASPAC 01). Lancet 2016;388(10041):248–57.
[3] Kamisawa T, Wood LD, Itoi T, Takaori K. Pancreatic cancer. Lancet 2016;388(10039):73–85.
[4] Shan T, Ma J, Ma Q, et al. β2-AR-HIF-1α: a novel regulatory axis for stress-induced pancreatic tumor growth and angiogenesis. Curr Mol Med 2013;13(6):1023–34.
[5] Duan W, Chen K, Jiang Z, et al. Desmoplasia suppression by metformin-mediated AMPK activation inhibits pancreatic cancer progression. Cancer Lett 2017;385:225–33.
[6] Hoffman RM, Bouvet M. Imaging the microenvironment of pancreatic cancer patient-derived orthotopic xenografts (PDOX) growing in transgenic nude mice expressing GFP, RFP, or CFP. Cancer Lett 2016;380(1):349–55.
[7] Boj SF, Hwang CI, Baker LA, et al. Organoid models of human and mouse ductal pancreatic cancer. Cell 2015;160(1–2):324–38.
[8] DeCant BT, Principe DR, Guerra C, Pasca dMM, Grippo PJ. Utilizing past and present mouse systems to engineer more relevant pancreatic cancer models. Front Physiol 2014;5:464.
[9] Morton JP, Timpson P, Karim SA, et al. Mutant p53 drives metastasis and overcomes growth arrest/senescence in pancreatic cancer. Proc Natl Acad Sci U S A 2010;107(1):246–51.
[10] Chen K, Qian W, Jiang Z, et al. Metformin suppresses cancer initiation and progression in genetic mouse models of pancreatic cancer. Mol Cancer 2017;16(1):131.
[11] Chen K, Qian W, Li J, et al. Loss of AMPK activation promotes the invasion and metastasis of pancreatic cancer through an HSF1-dependent pathway. Mol Oncol 2017;11(10):1475–92.
[12] Weidner N, Semple JP, Welch WR, Folkman J. Tumor angiogenesis and metastasis—correlation in invasive breast carcinoma. N Engl J Med 1991;324(1):1–8.
[13] Hruban RH, Adsay NV, Albores-Saavedra J, et al. Pathology of genetically engineered mouse models of pancreatic exocrine cancer: consensus report and recommendations. Cancer Res 2006;66(1):95–106.
[14] Rhim AD, Stanger BZ. Molecular biology of pancreatic ductal adenocarcinoma progression: aberrant activation of developmental pathways. Prog Mol Biol Transl Sci 2010;97:41–78.
[15] Nielsen SR, Quaranta V, Linford A, et al. Macrophage-secreted granulin supports pancreatic cancer metastasis by inducing liver fibrosis. Nat Cell Biol 2016;18(5):549–60.
[16] Wang X, Wei S, Zhao Y, et al. Anti-proliferation of breast cancer cells with itraconazole: hedgehog pathway inhibition induces apoptosis and autophagic cell death. Cancer Lett 2017;385:128–36.
[17] Binenbaum Y, Na'ara S, Gil Z. Gemcitabine resistance in pancreatic ductal adenocarcinoma. Drug Resist Updat 2015;23:55–68.
[18] Chen W, Zheng R, Baade PD, et al. Cancer statistics in China, 2015. CA Cancer J Clin 2016;66(2):115–32.
[19] Li X, Wang Z, Ma Q, et al. Sonic hedgehog paracrine signaling activates stromal cells to promote perineural invasion in pancreatic cancer. Clin Cancer Res 2014;20(16):4326–38.
[20] Feig C, Gopinathan A, Neesse A, Chan DS, Cook N, Tuveson DA. The pancreas cancer microenvironment. Clin Cancer Res 2012;18(16):4266–76.
[21] Tang D, Wang D, Yuan Z, et al. Persistent activation of pancreatic stellate cells creates a microenvironment favorable for the malignant behavior of pancreatic ductal adenocarcinoma. Int J Cancer 2013;132(5):993–1003.
[22] Tjomsland V, Niklasson L, Sandström P, et al. The desmoplastic stroma plays an essential role in the accumulation and modulation of infiltrated immune cells in pancreatic adenocarcinoma. Clin Dev Immunol 2011;2011:212810.
[23] Chu GC, Kimmelman AC, Hezel AF, DePinho RA. Stromal biology of pancreatic cancer. J Cell Biochem 2007;101(4):887–907.
[24] Neesse A, Algül H, Tuveson DA, Gress TM. Stromal biology and therapy in pancreatic cancer: a changing paradigm. Gut 2015;64(9):1476–84.
[25] Jones S, Zhang X, Parsons DW, et al. Core signaling pathways in human pancreatic cancers revealed by global genomic analyses. Science 2008;321(5897):1801–6.
[26] Gopinathan A, Morton JP, Jodrell DI, Sansom OJ. GEMMs as preclinical models for testing pancreatic cancer therapies. Dis Model Mech 2015;8(10):1185–200.
[27] Colvin EK, Scarlett CJ. A historical perspective of pancreatic cancer mouse models. Semin Cell Dev Biol 2014;27:96–105.
[28] Mann KM, Ying H, Juan J, Jenkins NA, Copeland NG. KRAS-related proteins in pancreatic cancer. Pharmacol Ther 2016;168:29–42.
[29] Weissmueller S, Manchado E, Saborowski M, et al. Mutant p53 drives pancreatic cancer metastasis through cell-autonomous PDGF receptor β signaling. Cell 2014;157(2):382–94.
[30] Hingorani SR, Petricoin EF, Maitra A, et al. Preinvasive and invasive ductal pancreatic cancer and its early detection in the mouse. Cancer Cell 2003;4(6):437–50.
[31] Hingorani SR, Wang L, Multani AS, et al. Trp53R172H and KrasG12D cooperate to promote chromosomal instability and widely metastatic pancreatic ductal adenocarcinoma in mice. Cancer Cell 2005;7(5):469–83.
[32] Rajabpour A, Rajaei F, Teimoori-Toolabi L. Molecular alterations contributing to pancreatic cancer chemoresistance. Pancreatology 2017;17(2):310–20.
[33] Chin V, Nagrial A, Sjoquist K, et al. Chemotherapy and radiotherapy for advanced pancreatic cancer. Cochrane Database Syst Rev 2018(3):CD011044.
[34] Amrutkar M, Gladhaug IP. Pancreatic cancer chemoresistance to gemcitabine. Cancers (Basel) 2017;9(11).
[35] Erstad DJ, Sojoodi M, Taylor MS, et al. Orthotopic and heterotopic murine models of pancreatic cancer and their different responses to FOLFIRINOX chemotherapy. Dis Model Mech 2018;11(7).
[36] Foucher ED, Ghigo C, Chouaib S, Galon J, Iovanna J, Olive D. Pancreatic ductal adenocarcinoma: a strong imbalance of good and bad immunological cops in the tumor microenvironment. Front Immunol 2018;9:1044.
[37] Yan X, Jiao SC, Zhang GQ, Guan Y, Wang JL. Tumor-associated immune factors are associated with recurrence and metastasis in non-small cell lung cancer. Cancer Gene Ther 2017;24(2):57–63.
[38] Zhang A, Qian Y, Ye Z, et al. Cancer-associated fibroblasts promote M2 polarization of macrophages in pancreatic ductal adenocarcinoma. Cancer Med 2017;6(2):463–70.
[39] Fan K, Yang C, Fan Z, et al. MUC16 C terminal-induced secretion of tumor-derived IL-6 contributes to tumor-associated Treg enrichment in pancreatic cancer. Cancer Lett 2018;418:167–75.
[40] Pushalkar S, Hundeyin M, Daley D, et al. The pancreatic cancer microbiome promotes oncogenesis by induction of innate and adaptive immune suppression. Cancer Discov 2018;8(4):403–16.